

Fiber-optical switch controlled by a single atom

Danny O'Shea, Christian Junge, Jürgen Volz, and Arno Rauschenbeutel*
*Vienna Center for Quantum Science and Technology, Atominstytut,
 Vienna University of Technology, 1020 Vienna, Austria*
 (Dated: June 17, 2022)

We demonstrate highly efficient switching of optical signals between two optical fibers controlled by a single atom. The key element of our experiment is a whispering-gallery mode bottle microresonator, which is coupled to a single atom and interfaced by two tapered fiber couplers. Even in the presence of the coupling fibers, the atom-resonator system reaches the strong coupling regime of cavity quantum electrodynamics (CQED), leading to a vacuum Rabi splitting in the excitation spectrum. We systematically investigate the switching efficiency of our system, i.e., the probability that the CQED fiber-optical switch redirects the light into the desired output. We obtain a large redirection efficiency reaching a raw fidelity of more than 60% without post-selection.

PACS numbers: 42.50.Pq, 42.50.Ct, 42.60.Da, 03.67.-a

Fiber-optical switches are devices that enable optical signals to be rerouted to different fiber output ports and play a vital role in today's optical communication networks. Scaling such a device into the quantum domain, where a single quantum system like an atom controls the flow of light, would enable the implementation of quantum communication protocols and quantum information processing with atoms and photons. Moreover, such a single-atom switch would enable the preparation of non-classical states of light that are useful for interferometric schemes in quantum metrology [1, 2].

The physical realization of such a quantum switch requires an enhanced light-matter interaction that can, e.g., be reached by coupling the atom to an optical microresonator. However, in order to switch the transmission and reflection of the resonator with a single atom, the so-called critical atom number, defined by $N_0 = 2\kappa\gamma/g^2$ [3], has to be much smaller than one. Here, κ and γ are the decay constants of the cavity field and the atomic dipole and g is the single photon-single atom coupling strength. This single-atom strong coupling regime in the optical domain has been investigated in numerous groundbreaking experiments using high finesse Fabry-Pérot microresonators [4–10]. These experiments clearly demonstrate the high potential of CQED systems for future applications. However, light absorption and scattering in the Fabry-Pérot mirrors limit the efficiency of coupling light into and out of the resonator to typically a few tens of percent. In order to move forward from these proof-of-principle studies, this optical loss thus has to be significantly reduced.

In this context, whispering-gallery-mode (WGM) microresonators combine very high atom-light coupling strengths [11–13] and low coupling losses in the same system. WGM resonators are monolithic dielectric structures, such as microspheres [14] and microtori [15], in which the light is guided near the surface by continuous total internal reflection [16]. The light can be coupled in and out by frustrated total internal reflection with

near 100% efficiency using tapered fiber couplers [17], thereby largely outperforming all other types of optical resonators.

Strong coupling of single atoms as well as of single solid state quantum emitters to WGM microresonators has recently been demonstrated in a number of experiments [18–24]. Moreover, using toroidal WGM microresonators, the basic functionality of a turnstile for photons has been implemented [21, 22]. In the latter experiments, the resonator was interfaced by a single coupling fiber and a weak incident classical light field was split into two counterpropagating streams of bunched and anti-bunched photons, respectively.

Here, we interface a WGM microresonator by two in-

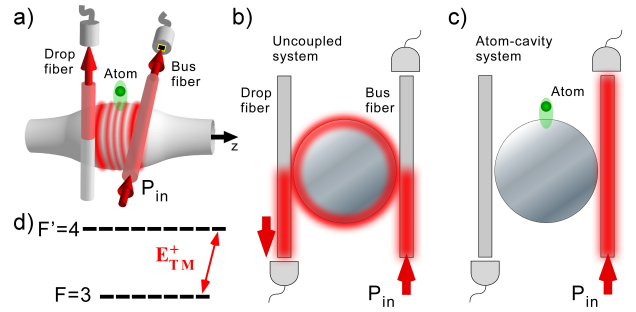


FIG. 1. Simplified experimental setup for the four-port optical switch. (a) Single ^{85}Rb atoms from an optical molasses couple to the TM-polarized evanescent field of a WGM bottle microresonator. Spectroscopy light with a power of $P_{\text{in}} \simeq 15 - 20$ photons/ μs couples into the resonator with an optical nanofiber (bus-fiber) and is transferred to the output port of a second nanofiber (drop-fiber) where it is detected by a single photon counter. (b,c) The presence or absence of an atom coupled to the evanescent field controls the flow of light between bus- and drop-fiber. (d) Excerpt from the ^{85}Rb level scheme with the Zeeman sublevels relevant for the experiment. The evanescent field of the counterclockwise rotating TM-polarized mode, E_{TM}^+ , is almost fully σ^+ -polarized. Thus, this light drives transitions from the $F = 3$, $m_F = 3$ ground state to the $F' = 4$, $m_{F'} = 4$ excited state (see text).

dependent coupling fibers and operate it in an add-drop configuration [25, 26]. Passive add-drop filters are used in optical communication for, e.g., wavelength-division multiplexing, where a given wavelength channel is unconditionally rerouted. In contrast, the add-drop filter realized in our experiment can be reconfigured by a single ^{85}Rb atom that controls the switching of light between the two fibers.

For our studies, we use a novel type of silica WGM microresonator, a so-called bottle microresonator [13, 27, 28]. It is conceptually similar to other WGM microresonators but has the additional advantage of being fully tunable. At the same time, it offers a highly advantageous mode-geometry that enables the simultaneous low-loss coupling to two tapered optical fibers with a nanofiber waist for in/out-coupling of light (see Fig. 1). This renders these resonators true four-port devices, ideally suited for the implementation of highly efficient, narrow-band add-drop filters [25, 26].

The operating principle of our switch is depicted in Fig. 1. The bottle microresonator in our experiment sustains WGMs with ultra-high quality factors ($Q \approx 5 \times 10^7$) as well as small mode volumes, thereby enabling operation in the strong coupling regime of CQED [24, 29]. Two nanofibers, called bus- and drop-fiber, are simultaneously coupled to the resonator mode with coupling constants κ_{bus} and κ_{drop} , respectively. We set the resonator-fiber distances such that the coupling constants for the bus-fiber fulfills the critical coupling condition $\kappa_{\text{bus}} = \sqrt{(\kappa_i + \kappa_{\text{drop}})^2 + h^2}$ [25], where $\kappa_i = 2\pi \times 4.8$ MHz is the intrinsic loss-rate and $h = 2\pi \times 1.7$ MHz is the backscattering rate of the resonator mode. Due to the low backscattering of our resonator mode, we can neglect h in the following. The total decay rate of the resonator field is given by $\kappa = \kappa_i + \kappa_{\text{bus}} + \kappa_{\text{drop}}$.

With these settings, we obtain the situation illustrated in Fig. 1 (b), where ideally all light that is incident through the bus-fiber is resonantly coupled into the resonator and the remaining bus-fiber transmission, T_{bus}^0 , is zero. At the same time, a large fraction of the light is out-coupled from the resonator and transmitted into the drop fiber. This situation corresponds to the ON-state of the switch. In order to prepare the OFF-state of the switch, a modification of the resonance frequency of the resonator is required. This can be realized in the strong coupling regime by a single atom in the resonator mode, whose presence prevents the build up of the resonator field. In this case, all incident light remains in the bus fiber [see Fig. 1 (c)].

In order to demonstrate this scheme in our experiment, we tune the bottle microresonator and the probe light into resonance with the atomic transition $5S_{1/2}, F = 3 \rightarrow 5P_{3/2}, F' = 4$ of ^{85}Rb (wavelength $\lambda = 780$ nm) and set the power of the incident light such that the mean intra-resonator photon number is $n_{\text{cav}} \approx 0.10$ for the empty resonator. We choose the polarization of the

probe light in the bus-fiber such that it couples into the TM-polarized resonator mode. In this case, due to the presence of a strong longitudinal electric field component, the clockwise (counterclockwise) propagating resonator mode is nearly perfectly σ^- (σ^+) polarized, with respect to the quantization axis defined by the resonator fiber [see z-axis in Fig. 1(a)]. In our experiment, we probe the counterclockwise propagating mode and optically pump the atom into the $F = 3, m_F = 3$ Zeeman sublevel. As a consequence, the σ^+ -polarized cavity field excites the atom on the cycling transition to the state $F' = 4, m_F = 4$, from which it can only decay back to the original ground state [see Fig. 1(d)]. The photon emitted in the following decay is again σ^+ -polarized, and thus, the atom exclusively interacts with σ^+ -polarized counterclockwise propagating mode. Despite the simultaneous existence of two degenerate resonator modes, this effectively leads to the ideal case of a two-level atom that only interacts with a single traveling-wave mode [24].

In order to couple atoms to the resonator, our setup is mounted in an ultra-high vacuum chamber in which a 1-cm diameter cloud with 5×10^7 laser-cooled atoms is delivered to the resonator using an atomic fountain. Figure 2 displays the time-dependent transmissions T_{bus} and T_{drop} through the bus and drop fiber, respectively, when an atom passes through the resonator mode. When the atom-resonator coupling becomes significant, the incoming light field is prevented from entering the resonator and remains in the bus-fiber. We thus observe a concomitant increase (decrease) in bus- (bus-to-drop-) fiber transmission, see Fig. 2. The temporal width of this transit signal of around $5 \mu\text{s}$ is consistent with the expected transit time for an atom with a thermal velocity corresponding to the $5 \mu\text{K}$ -temperature of the atom cloud. In order to obtain reproducible experimental conditions on

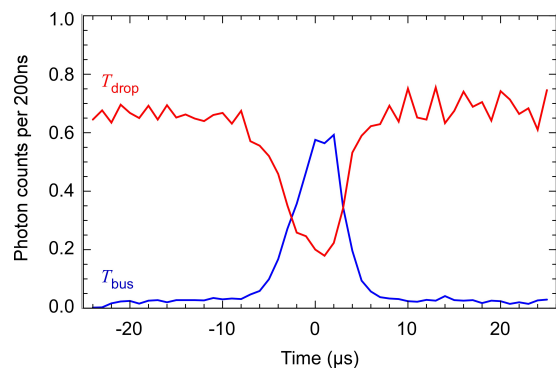


FIG. 2. On-resonance bus-fiber and bus-to-drop-fiber transmission (timebin: 200 ns) during the transit of an atom through the resonator mode, for the same experimental setting as in Fig. 3. The plotted data shows the transmission signal averaged over 294 single atom transits. The centers of mass of the individual transmission signals are aligned to $t = 0 \mu\text{s}$.

this time scale, an FPGA-based real-time detection and experimental control system reacts to the presence of an atom in the resonator mode with around 160 ns response time [24, 29]

We use our real-time control system in order to perform spectroscopy on the coupled atom-resonator system by scanning the frequency ω_l of the probe laser across the common resonator and atom resonance frequency $\omega_r = \omega_a$. Figure 3 shows the transmission spectra measured at both output ports as a function of the resonator-laser detuning $\Delta\omega_{rl} = \omega_r - \omega_l$. The blue \blacklozenge (red \blacksquare) mark the bus- (bus-to-drop-) fiber transmission with an atom coupled to the resonator mode, while the green \blacktriangle (grey \bullet) represent the transmission after removing the atom from the resonator mode [see inset Fig. 3]. We clearly observe an atom-induced splitting of the transmission spectrum into two distinct peaks, the so-called vacuum-Rabi splitting [3]. This experimentally demonstrates that it is possible to strongly couple single atoms to a whispering-gallery mode resonator in add-drop configuration while maintaining a high on-resonance photon survival probability of $\approx 60\%$

In order to infer the atom-resonator coupling strength for this dataset, we numerically solve the Master equation of the Jaynes-Cummings Hamiltonian, taking into account the full Zeeman substructure of the atom as well as the full vectorial description of the evanescent electric field of the two counter-propagating WGM modes (see Ref. [24] for details). In order to account for the motion of the atom and the resulting distribution of coupling constants, we solve the Master equation for a set of coupling strengths in the interval $g/2\pi = 7.5$ MHz to 30 MHz and subsequently fit a normally distributed sum of these spectra to the data. For this fit, the mean coupling constant \bar{g} and the standard deviation σ_g are the only free parameters. The theoretical spectra obtained in this way are the solid lines in Fig. 3 and show good agreement with our experimental data for $\bar{g}/2\pi = 15$ MHz and $\sigma_g = 9$ MHz. The maximum switching contrast is on resonance ($\Delta\omega_{rl} = 0$), where the measurement yields a 10 dB increase in bus-fiber transmission from around 3% in the ON-state to 46% in the OFF-state and a 7 dB decrease in bus-to-drop fiber transmission from 58% in the ON-state to 12 % in the OFF-state of the switch.

In order to find the optimal operating conditions of the switch, we scan the distance between resonator and the drop-fiber while maintaining critical coupling for the bus-fiber. We measure the on-resonance transmission to both output ports as a function of the total cavity decay rate κ for the case of an atom coupled to the resonator [blue \blacklozenge and red \blacksquare in Fig. 4 (a)] as well as for the uncoupled case [grey \bullet and green \blacktriangle in Fig. 4 (a)]. As expected, the effect of the atom decreases with increasing resonator decay rate κ due to the reduction of the single atom cooperativity of the atom-resonator system. This can be seen in the monotonous increase (decrease) of the

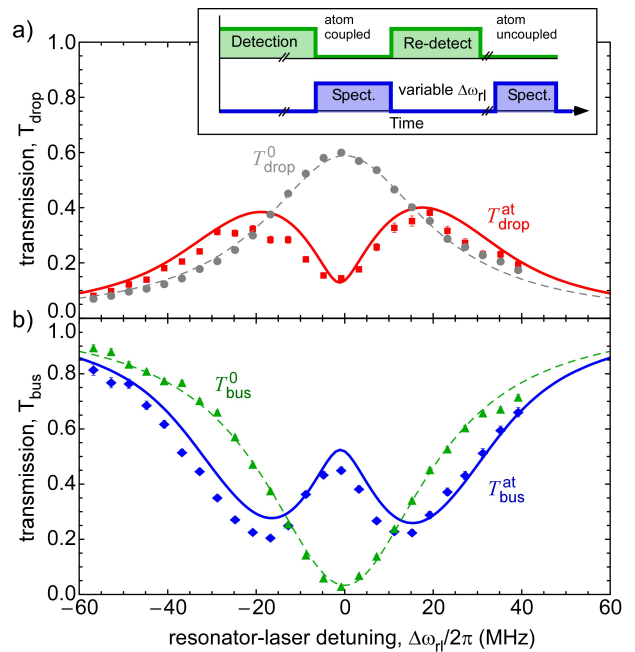


FIG. 3. Normalized transmission spectra of the atom-resonator system measured a) through the bus-fiber (T_{bus}) and b) from bus- to drop-fiber (T_{drop}) as a function of resonator-laser detuning $\Delta\omega_{rl}$. The data for the coupled atom-resonator system $T_{\text{bus}}^{\text{at}}$ and $T_{\text{drop}}^{\text{at}}$ is represented by the blue (\blacklozenge) and red (\blacksquare) data points, respectively. The data for the uncoupled case T_{bus}^0 and T_{drop}^0 is shown in grey (\bullet) and green (\blacktriangle), respectively, and the dashed lines are Lorentzian fits. The solid lines are obtained from a theoretical fit to the data using an extended Jaynes-Cummings model to include the full properties of WGM resonator modes. The fit yields a mean coupling strength $\bar{g}/2\pi = 15.6$ MHz. The error bars indicate the $\pm 1\sigma$ statistical error. The residual difference between experimental data and theoretical prediction possibly originates from a misalignment of the magnetic guiding field with respect to the resonator axis which would limit the efficiency of optically pumping the atom into the $F = 3$, $m_F = 3$ Zeeman sublevel (see text).

bus-to-drop- (bus-) fiber transmission $T_{\text{drop}}^{\text{at}}$ ($T_{\text{bus}}^{\text{at}}$) with κ . At the same time, in the uncoupled case, the bus-to-drop-fiber transmission T_{drop}^0 increases monotonously in good agreement with the expected theoretical prediction $T_{\text{drop}}^0 = 1 - 2(\kappa_i/\kappa)$ (solid line) [12] and the remaining transmission through the bus-fiber T_{bus}^0 is approximately zero.

We quantify the switching process by calculating the classical fidelity $\mathcal{F} = 1/2(T_{\text{bus}}^{\text{at}} + T_{\text{drop}}^0)$ of the process, i.e., the raw probability that a single input photon will be routed into the correct fiber port, without correcting for photon loss. This fidelity is given by the orange data (o) shown in Fig. 4 (b) and is maximal for resonator linewidths between $\kappa \simeq 30$ –50 MHz. In this range, we find a remarkably constant bus fiber transmission of $T_{\text{bus}}^{\text{at}} \simeq 45$ –55% despite a large increase in the cavity decay rate. For optimum settings of the resonator-

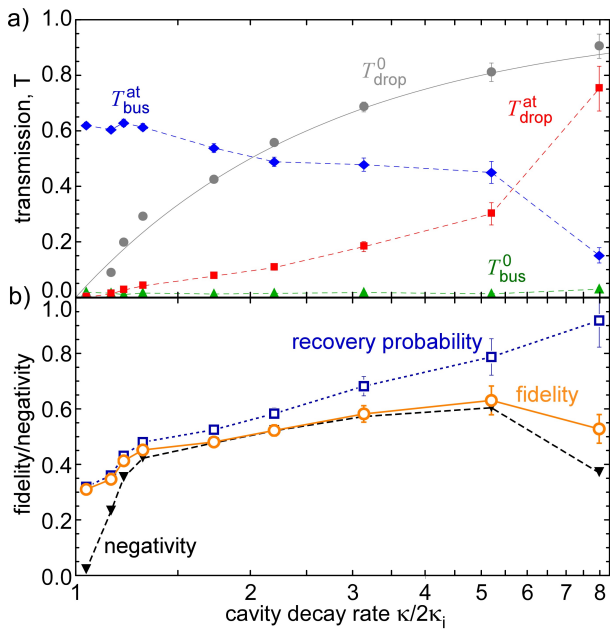


FIG. 4. (a) Measurements of the on-resonance transmission $T_{\text{bus}}^{\text{at},0}$ (blue \blacklozenge , green \blacktriangle) and $T_{\text{drop}}^{\text{at},0}$ (red \blacksquare , grey \bullet) as a function of the resonator decay rate κ . The dashed lines are a guide to the eye, and the solid line is given by $T_{\text{drop}}^0 = 1 - 2(\kappa_i/\kappa)$ (see text). (b) Fidelity of the switch operation (orange \circ) and probability to recover an incident photon (blue \square) inferred from the data in (a). The error bars indicate the $\pm 1\sigma$ statistical error and the lines are guides to the eye. The black data (\blacktriangledown) is the expected negativity for the generation of an entangled Bell state when a ^{85}Rb atom is prepared in a superposition between the two hyperfine ground states, assuming a fully coherent atom switching process as described in the main text.

fiber coupling, we find a fidelity of $\mathcal{F} = 0.62$ and, at the same time, there is a 79% probability to recover an incident photon after the switching operation. We note that the maximum fidelity is not achieved in the strong coupling regime but at the crossover to the regime where the atom–light coupling rate g is smaller than the resonator decay rate κ , but still dominates over the spontaneous emission rate of the atom γ . Thus, the underlying switching mechanism is robust against experimental variations in κ as long as the condition $g^2/\kappa\gamma > 1$ is satisfied.

A multi-port optical switch that is controlled by a single atom is a powerful tool for future quantum applications such as in quantum networks. In particular, the atom could be prepared in a (equal) superposition between two internal ground states, e.g., the two hyperfine ground states $F = 2$ and $F = 3$ of ^{85}Rb , where only one of them interacts with the resonator. In this case, after the interaction of the switch with an incident photon, the atom–photon system will ideally end up in a maximally entangled Bell-state. Thus, a quantum switch facilitates the deterministic entanglement between two initially independent quantum systems. Assuming a coherent inter-

action between the incident light and the atom-resonator system — which should be possible using weak input light powers and slowly varying pulse envelopes ($\sim 0.1 \mu\text{s}$ for our experimental parameters) — we can calculate the expected performance of our system for the deterministic generation of matter–light entanglement. Under this assumption, one would obtain the same fidelity as measured here for the classical case [orange \circ in Fig. 4 (b)]. To better quantify the amount of entanglement that can be produced, we calculate the corresponding negativity [30] of the final atom–photon state for each measurement [black \blacktriangledown in Fig. 4 (b)]. Even including the photon loss, we obtain a maximum value of around 0.6.

In summary, we demonstrate highly efficient switching of optical signals, where a single atom coupled to a bottle microresonator controls the output port of an incident light field. The switching fidelity of more than $\mathcal{F} = 0.62$ in conjunction with the low optical losses – around 79% of the incident photons are recovered – illustrates the potential of this system for future applications under realistic conditions. In particular, the high degree of light–matter entanglement expected for such a system would render it a powerful tool for many fiber-based quantum information and communication applications. Moreover, the low intrinsic losses would enable the on-demand generation of Schrödinger cat-like entangled states containing many photons. These quantum states are an essential resource for quantum metrology applications [1, 2].

The expected switching fidelity of our bottle-microresonator system can be further improved by reducing the motion of the atoms. Trapping the atoms close to the resonator surface using a nanofiber-based dipole trap [31] would strongly reduce the fluctuations in the coupling rate g and would yield a significantly more stable operation of the switch. Furthermore, experiments show that it is possible to increase the quality factor of the bottle microresonator by at least a factor of five [28]. With these improvements and assuming realistic trapping conditions, a deterministic generation of matter–light entanglement with a fidelity/negativity of more than 95% is within reach, thereby enabling a realm of possible applications in quantum science and technology.

We gratefully acknowledge financial support by the European Science Foundation, the Volkswagen Foundation, and the Austrian Science Fund (FWF; SFB FoQuS Project No. F 4017). J.V. acknowledges support by the European Commission (Marie Curie IEF Grant 300392). C.J. acknowledges support by the German National Academic Foundation.

* Arno.Rauschenbeutel@ati.ac.at

[1] V. Giovannetti, S. Lloyd, and L. Maccone, *Science* **306**,

- 1330 (2004).
- [2] V. Giovannetti, S. Lloyd, and L. Maccone, *Nat Photon* **5**, 222 (2011).
- [3] P. R. Berman, *Cavity quantum electrodynamics* (Academic Press, Inc., Boston, 1994).
- [4] K. M. Birnbaum, A. Boca, R. Miller, A. D. Boozer, T. E. Northup, and H. J. Kimble, *Nature* **436**, 87 (2005).
- [5] A. D. Boozer, A. Boca, R. Miller, T. E. Northup, and H. J. Kimble, *Phys. Rev. Lett.* **98**, 193601 (2007).
- [6] T. Wilk, S. Webster, A. Kuhn, and G. Rempe, *Science* **317**, 488 (2007).
- [7] M. L. Terraciano, R. Olson Knell, D. G. Norris, J. Jing, A. Fernandez, and L. A. Orozco, *Nat. Phys.* **5**, 480 (2009).
- [8] T. Kampschulte, W. Alt, S. Brakhane, M. Eckstein, R. Reimann, A. Widera, and D. Meschede, *Phys. Rev. Lett.* **105**, 153603 (2010).
- [9] J. Volz, R. Gehr, G. Dubois, J. Esteve, and J. Reichel, *Nature* **475**, 210 (2011).
- [10] S. Ritter, C. Nolleke, C. Hahn, A. Reiserer, A. Neuzner, M. Uphoff, M. Mucke, E. Figueroa, J. Bochmann, and G. Rempe, *Nature* **484**, 195 (2012).
- [11] J. R. Buck and H. J. Kimble, *Phys. Rev. A* **67**, 033806 (2003).
- [12] S. M. Spillane, T. J. Kippenberg, K. J. Vahala, K. W. Goh, E. Wilcut, and H. J. Kimble, *Phys. Rev. A* **71**, 013817 (2005).
- [13] Y. Louyer, D. Meschede, and A. Rauschenbeutel, *Phys. Rev. A* **72**, 031801 (2005).
- [14] V. Braginsky, M. Gorodetsky, and V. Ilchenko, *Phys. Lett. A* **137**, 393 (1989).
- [15] D. K. Armani, T. J. Kippenberg, S. M. Spillane, and K. J. Vahala, *Nature* **421**, 925 (2003).
- [16] A. Matsko and V. Ilchenko, *Selected Topics in Quantum Electronics*, *IEEE Journal of* **12**, 3 (2006).
- [17] S. M. Spillane, T. J. Kippenberg, O. J. Painter, and K. J. Vahala, *Phys. Rev. Lett.* **91**, 043902 (2003).
- [18] T. Aoki, B. Dayan, E. Wilcut, W. P. Bowen, A. S. Parkins, T. J. Kippenberg, K. J. Vahala, and H. J. Kimble, *Nature* **443**, 671 (2006).
- [19] Y. Park, A. Cook, and H. Wang, *Nano Lett.* **6**, 2075 (2006).
- [20] K. Srinivasan and O. Painter, *Nature* **450**, 862 (2007).
- [21] B. Dayan, A. Parkins, T. Aoki, E. Ostby, K. Vahala, and H. Kimble, *Science* **319**, 1062 (2008).
- [22] T. Aoki, A. S. Parkins, D. J. Alton, C. A. Regal, B. Dayan, E. Ostby, K. J. Vahala, and H. J. Kimble, *Phys. Rev. Lett.* **102**, 083601 (2009).
- [23] D. J. Alton, N. P. Stern, T. Aoki, H. Lee, E. Ostby, K. J. Vahala, and H. J. Kimble, *Nat. Phys.* **7**, 159 (2010).
- [24] C. Junge, D. O'Shea, J. Volz, and A. Rauschenbeutel, *Phys. Rev. Lett.* **110**, 213604 (2013).
- [25] H. Rokhsari and K. J. Vahala, *Phys. Rev. Lett.* **92**, 253905 (2004).
- [26] M. Pöllinger and A. Rauschenbeutel, *Opt. Express* **18**, 17764 (2010).
- [27] M. Sumetsky, *Opt. Lett.* **29**, 8 (2004).
- [28] M. Pöllinger, D. O'Shea, F. Warken, and A. Rauschenbeutel, *Phys. Rev. Lett.* **103**, 053901 (2009).
- [29] D. O'Shea, C. Junge, M. Poellinger, A. Vogler, and A. Rauschenbeutel, *Appl. Phys. B* **105**, 129 (2011).
- [30] G. Vidal and R. F. Werner, *Phys. Rev. A* **65**, 032314 (2002).
- [31] E. Vetsch, D. Reitz, G. Sagué, R. Schmidt, S. T. Dawkins, and A. Rauschenbeutel, *Phys. Rev. Lett.* **104**, 203603 (2010).